



Effective adsorption of Co^{2+} and Sr^{2+} ions by 10-tungsten-2-molybdophosphoric acid supported amine modified magnetic SBA-15

Hanieh Fakhri¹ · Ali Reza Mahjoub¹ · Hassan Aghayan²

Received: 9 March 2019 / Published online: 10 July 2019
© Akadémiai Kiadó, Budapest, Hungary 2019

Abstract

The presence of heavy metals in water sources have created serious environmental concerns. In this study, 10-tungsten-2-molybdophosphoric acid supported amine-functionalized magnetic SBA-15 with core–shell morphology was prepared and its applicability as effective inorganic adsorbent for Co^{2+} and Sr^{2+} removal was investigated. The adsorbent was characterized by X-ray powder diffraction, Fourier transform infrared spectroscopy, transmission electron microscopy, scanning electron microscopy, vibrating sample magnetometer, inductively coupled plasma analysis and N_2 physical adsorption–desorption technique. The effective parameters including dosage of adsorbent, contact time, initial concentration of metal ion, pH of solution, temperature and elution agent were investigated. Batch adsorption studies depicted higher adsorption affinity for Co^{2+} than Sr^{2+} ions. The synthesized adsorbent has an adsorption capacity of 87.72 mg g^{-1} and 80.01 for Co^{2+} and Sr^{2+} respectively. This research highlights the source of difference between their adsorption capacity. EDTA had more desorption performance as elution agent than HCl that attributed to larger chelating stability constant of EDTA. Moreover, the results showed the good recyclability and excellent stability of adsorbent after 4 successive cycles.

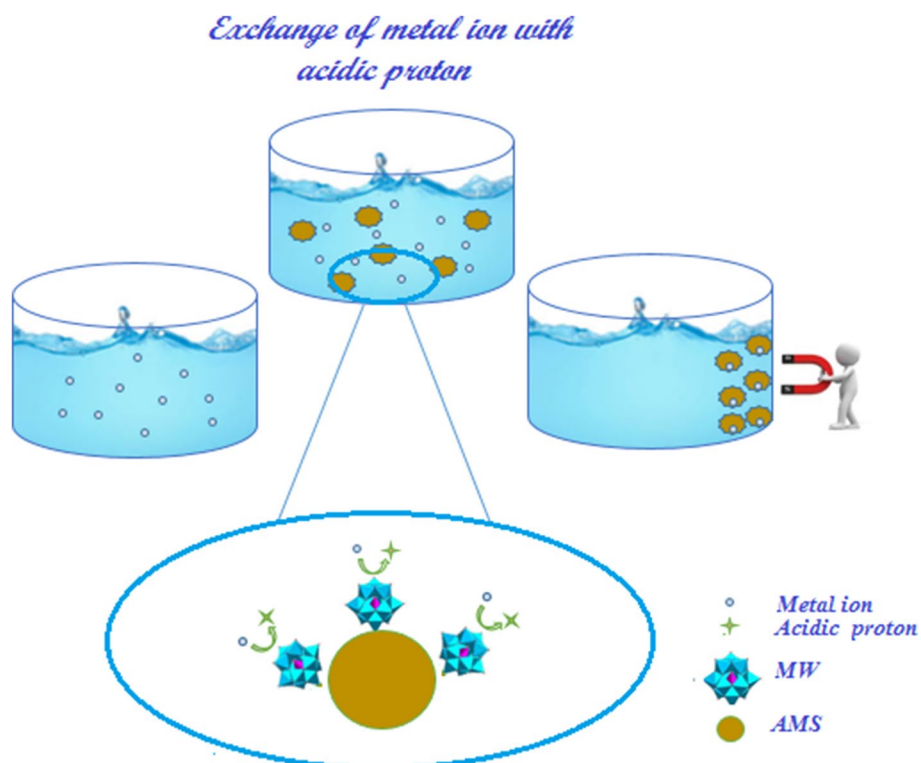
Electronic supplementary material The online version of this article (<https://doi.org/10.1007/s10967-019-06595-6>) contains supplementary material, which is available to authorized users.

✉ Ali Reza Mahjoub
Mahjouba@modares.ac.ir
Hanieh Fakhri
hanieh_fakhrie@yahoo.com

¹ Department of Chemistry, Tarbiat Modares University, P.O. Box. 14155-4383, Tehran, Iran

² Material and Nuclear Fuel Research School, Nuclear Science and Technology Research Institute (NSTRI), P.O. Box. 11365-8486, Tehran, Iran

Graphic abstract



Keywords Heteropoly acid · Magnetic SBA-15 · Cobalt adsorption · Strontium adsorption

Introduction

Universal industrialization, population growth and natural activities discharge high volume of heavy metals into environmental sources that have created serious concern [1, 2]. Cobalt (Co) and strontium (Sr) as major components of the toxic group have great solubility in aquatic system [3] and especially their presence in radioactive wastewaters has doubled this concern. These metals are non-biodegradable and can accumulate in living organisms. More and more usage from Co and Sr resources and the absence of a comprehensive pattern for management of these wastes lead to the uncontrolled release of these metals [4] which can be effected on human health as paralysis, various cancer, lung discomfort and bone defects [5]. According to regulations of Agency for Toxic Substances and Disease Registry, the maximum allowed value is $2 \mu\text{g L}^{-1}$ for cobalt ion [6] and presence of its higher value induces critical problems. In the other hand, strontium with similar ion radius with calcium can easily exchange with it in bone issue and create cancer and other diseases. So nowadays, effective removal of them is considered as hot environmental research subject. Chemical oxidation, filtration, chemical precipitation,

photolysis, reverse osmosis, electro chemical process and etc. are common technologies that applied to treatment of polluted solution [7]. However, these strategies are very expensive and mostly useless when concentrations of metal ion in solution are less than 100 mg L^{-1} [8, 9]. Adsorption is efficient and economic method because of its easy operation, accessibility of various adsorbent and good selectivity. In the recent years, heteropoly acids (HPAs) introduced as green inorganic adsorbent for water treatment [10, 11]. HPAs are a unique type of inorganic metal–oxide clusters with excellent acidic properties which provide exchangeable hydrogen ions when they are soaked in the aqueous solution [12]. However, low surface area and solubility in polar solution confine usage of HPAs. Many efforts have focused on immobilizing HPAs onto various supports such as silica [13, 14], zeolites [15], graphene oxide [16, 17] and etc. Silica is considered as desire support due to its high surface areas, good porous channels, narrow pore size distributions and the plenty silanol groups at the surface of its channels [18]. Masteri-Farahani and Modarres [19] reported excellent catalytic performance of HPAs supported surface modified SBA-15. In the other study, improved ion exchange capability is achieved by ammonium salt of hetropoly acid

supporting on mesoporous silica that investigated by Park et al. [20]. Nevertheless, adsorbent separation from the solution at the end of the adsorption process will still remain as another challenge. To address this issue, fabrication of magnetic adsorbents can be considered as excellent idea owing to quickness, eco-friendliness, easy handling of magnetic material [21, 22]. In this study, core-shell magnetic support containing a magnetic nanoparticle core and silica shell are prepared for supporting HPAs. Core-shell structure is selected for four main reasons: First, the outer mesoporous SBA-15 shell with more free sites can easily be functionalized by other functional groups; Second, magnetic nanoparticle cores are protected from oxidized by the surrounding environment, Third, less blocking of pore is happened when magnetic nanoparticles are as a core structure, Forth, leaching of magnetic nanoparticles into a low pH medium is stopped. Furthermore, decoration of magnetic support with amine-functional groups leads to better grafting of HPAs on the surface of support and also increases tendency for more loading of HPAs resulting in producing stable and strong adsorbents. In this study, we immobilized HPAs on amine-functionalized magnetic SBA-15 (AMS) and characterized it by various measurements. In the following, our study focused on adsorption experiments with five main aspects: (1) to investigate adsorption capacity of adsorbent for Co^{2+} and Sr^{2+} adsorption, (2) To examine various effective parameters on adsorption process such as pH, contact time, amount of adsorbent, initial concentration of heavy metal and temperature, (3) to describe possible mechanisms of adsorption, (4) to assay effect of elution agent on desorption efficiency, (5) to evaluate recyclability performance of adsorbent.

Experimental

Materials

All of these chemicals were used without further purification. $\text{FeCl}_3 \cdot 6\text{H}_2\text{O}$, polyethylene glycol, sodium acetate ($\text{NaAc} \cdot 3\text{H}_2\text{O}$), ethylene glycol (EG), Ammonium hydroxide (NH_4OH , 28 wt%), tetraethyl orthosilicate (TEOS, 98%), absolute ethanol (99.98%), sodium molybdate ($\text{Na}_2\text{MoO}_4 \cdot 2\text{H}_2\text{O}$), sodium tungstate ($\text{Na}_2\text{WO}_4 \cdot 2\text{H}_2\text{O}$), disodium hydrogenphosphate (Na_2HPO_4), Cetyl trimethylammonium bromide (CTAB, $\text{C}_{19}\text{H}_{42}\text{BrN}$), diethyl ether ($(\text{C}_2\text{H}_5)_2\text{O}$), sulfuric acid (H_2SO_4 98%), 3-amino propyl trimethoxy silane (APTMS) and toluene were purchased from Merck and Sigma-Aldrich Company.

Synthesis of AMS support

The magnetite nanospheres were synthesized by using the solvothermal method [23]. According to the procedure, the

mixture including 1.2 g of $\text{FeCl}_3 \cdot 6\text{H}_2\text{O}$, 1.0 g of polyethylene glycol and 3.3 g of $\text{NaAc} \cdot 3\text{H}_2\text{O}$ were added to 50 mL of EG and stirred for 30 min at room temperature. So, the resultant solution was transferred to Teflon-lined stainless steel autoclave and heated at 200 °C for 8 h. Finally, the obtained solid was filtered, washed with ethanol and dionized water and dried at 60 °C for 12 h. This magnetic product is donated as M. Subsequently, the following procedure is applied for preparing of magnetic core-shell silica [24]. Typically, 2 g of obtained M was dissolved in a mixture of solvents containing absolute ethanol, distilled water and NH_4OH with ratio 26:6:1. These solution was sonicated for 10 min. In the next step, TEOS (6 mL) was added to it and stirred at 40 °C for 1 h. Subsequently, 1.8 g CTAB as the structure-directing agent was added to it. Then, the solution was refluxed for 22 h. Finally, the powder was filtered by an external magnetic field and washed with ethanol and dionized water, dried in a vacuum oven at 50 °C for 12 h and calcined for 6 h at 300 °C. This product is donated as MS.

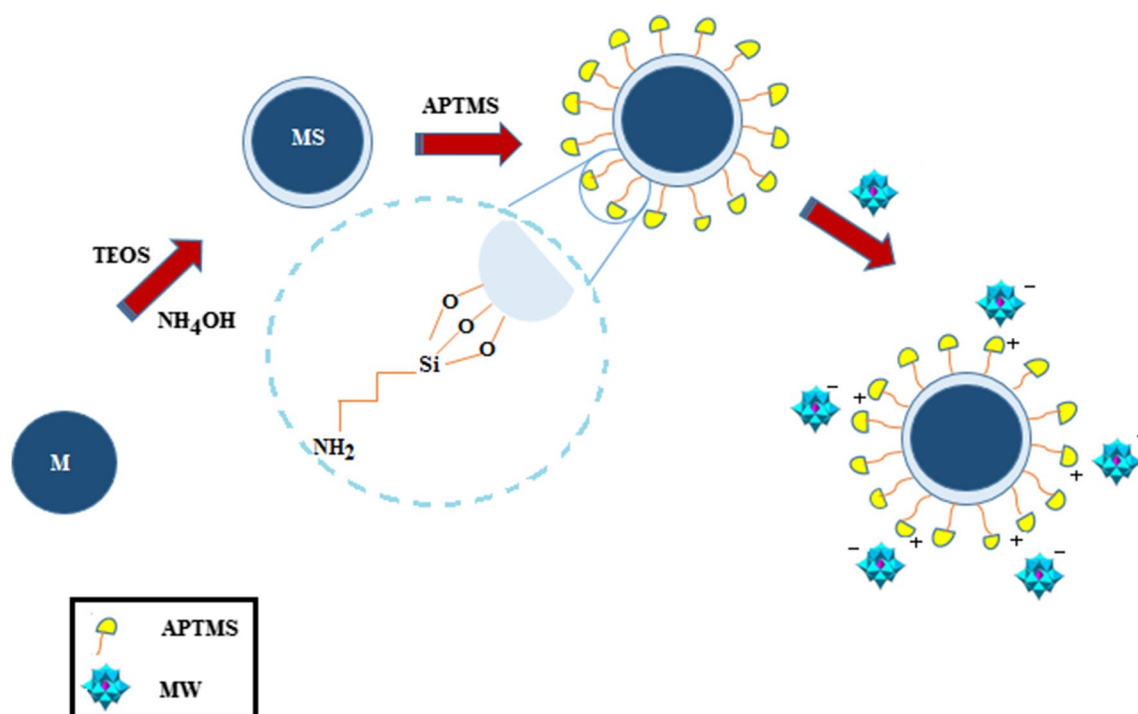
The modification of the external surface of MS with amine groups was performed by using APTMS. For this purpose, 2 g of MS was dispersed in certain volume of toluene and 3 mmol of APTMS was added to it. The obtained mixture was refluxed for 20 h. Then the resultant solid was separated by external magnetic field and washed with dionized water and ethanol and finally was dried at 60 °C for 12 h. The as-synthesized adsorbent is denoted as AMS.

Synthesis of MW@AMS nanocomposite

The kegging type heteropoly acid with overall formula $\text{H}_3[\text{PMo}_2\text{W}_{10}\text{O}_{40}] \cdot n\text{H}_2\text{O}$ (MW) was synthesized via reported procedure [25]. The defined amounts of MW species were dispersed in distilled water and AMS support was added to it. This sealed mixture was stirred at 110 °C for 24 h. In the following, the mixture was unsealed and stirred at room temperature until the solvent is evaporated. Finally, the collected powder was dried at 120 °C and calcined at 300 °C for 4 h. This adsorbent is denoted as MW@AMS. ICP analysis indicated that the atomic ratios of P/Mo/W were: 1.00/1.79/9.68. This procedure was employed for preparation of various loading of MW on the support. The applied steps for the synthesis of this adsorbent are indicated in Scheme 1.

Characterization

X-ray diffraction analysis (XRD) was carried out by Philips X-pert X-ray diffractometer and Cu $\text{K}\alpha$ radiation (wavelength, $\lambda = 1.5481 \text{ \AA}$) was used as the radiation source. The morphology and textural structures were assayed by scanning electron microscopy (Philips XL-300 instrument) and transmission electron microscopy (Philips cm 30). The Fourier transform infrared spectroscopy (FT-IR) spectra of the synthesized



Scheme 1 The overall steps applied for preparing of MW@AMS

samples were characterized by the Shimadzu-8400S spectrometer. ICP (Varian vista-PRO instrument) analysis recorded metal ion concentration at various times. The magnetization measurement was obtained by vibrating sample magnetometer (Lake Shore 7410 VSM) at room temperature. Nova Station A instrument at 77 K was applied for measuring of N₂ adsorption–desorption isotherms. Specific surface areas were determined by the Brunauer–Emmet–Teller (BET) method and the Barrett–Joyner–Halenda (BJH) method were used for calculation of the pore-size distribution.

Adsorption experiments

Adsorption assays were performed using 50 mg of adsorbent per 20 mL of metal solution (desired concentration) under stirring. After specific time intervals, the solid phase was filtered by external magnet and the remained metal ion concentration in the liquid phase was monitored by ICP elemental analysis. The stock solutions containing Co²⁺ and Sr²⁺ ions were prepared of CoSO₄·7H₂O and Sr(NO₃)₂·4H₂O respectively. The effect of solution pH (pH = 1–13), contact time ($t=0$ –180 min), initial metal concentration ($C_0=10$ –200 ppm) and elution solution were investigated. The Eqs. 1 and 2 are employed for determining of the adsorption capacity and removal efficiency respectively.

$$\text{Adsorption capacity} = \frac{(C_0 - C_e)V}{m} \quad (1)$$

$$\% \text{Removal efficiency} = \frac{C_0 - C_e}{C_0} * 100 \quad (2)$$

where C_0 (mg L⁻¹) and C_e (mg L⁻¹) are concentration of metal ion in liquid phase at initial and equilibrium time respectively; V (L) is total volume of solution and m (g) is mass of adsorbent.

Result and discussion

Characterizations of adsorbent

The crystalline structure and purity phase of samples depicted in Fig. 1. In Fig. 1a, the diffraction peaks showed inverse spinel crystalline structure with cubic symmetry of M (JCPDS Number: 79-0418) [26]. Furthermore, the existence of these diffractions is preserved after coating with silica and MW as presented in Fig. 1b, c. The absence of the reflection peaks related to MW (Fig. 1d) in MW@AMS pattern was a result of high dispersion of immobilized species on the modified support (Fig. 1c) [27]. A strong peak at $2\theta=0.53^\circ$ was observed in low angle XRD patterns of AMS (Fig. 1e) that can be assigned to (100) plane. For MW@AMS sample, this reflection was remained while the peak intensity diminished. This is corresponded to the reduction in arrangement of mesoporous channels of silica along with incorporation of MW species.

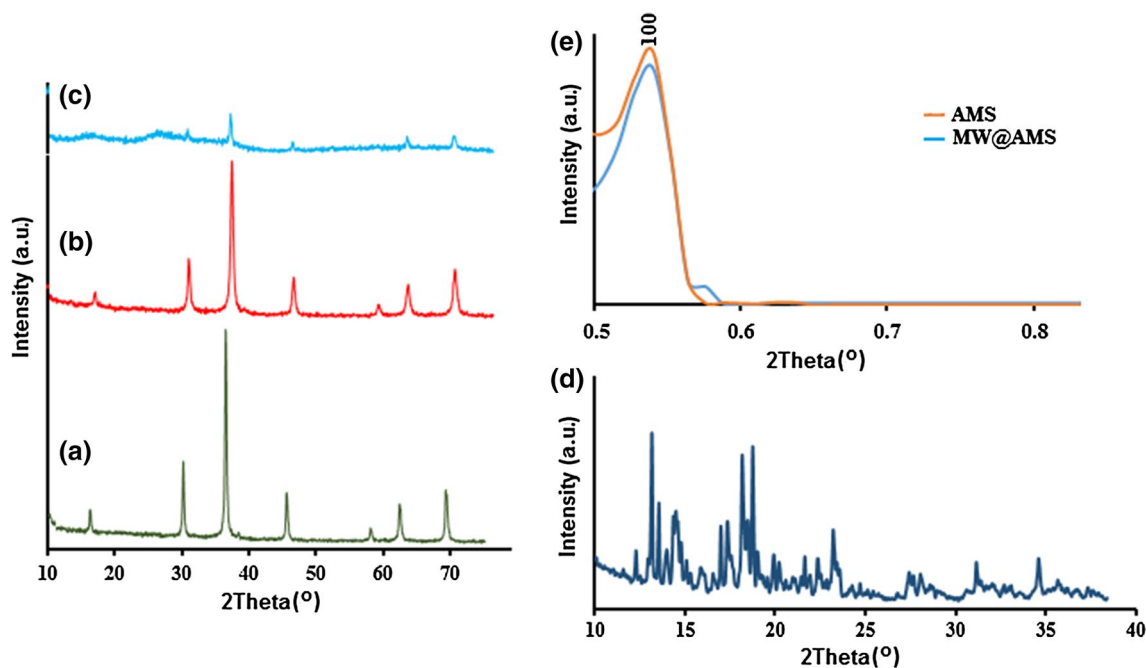


Fig. 1 High-angle XRD patterns of M (a), AMS (b), MW@AMS (c), MW (d) and low-angle XRD pattern of AMS and MW@AMS (e)

The FT-IR analysis was applied for investigation about structure and interactions of synthesized adsorbent (Fig. 2). The broad and strong band at $3000\text{--}3600\text{ cm}^{-1}$ for all samples assigned to O–H stretching mode while the sharper band at 1618 cm^{-1} is related to the deformation vibration of free water molecules [28]. The characteristic band at 562 cm^{-1} is attributed to Fe–O bond stretching (Fig. 2a) [29]. In Fig. 2b, the observed peaks at 1076 cm^{-1} and 801 cm^{-1} can be corresponded to the asymmetric and symmetric stretching vibrations of Si–O–Si and the band at 471 cm^{-1} is attributed to the Si–O–Si or O–Si–O bending mode of SiO_2 [24]. Following the functionalization of MS by amine group, two main peaks are observed at 3416 cm^{-1} and 1533 cm^{-1} which referred to stretching and bonding vibrations of N–H group respectively (Fig. 2b) [30]. The observed adsorption peak at $2800\text{--}2989\text{ cm}^{-1}$ is assigned to stretching vibration of methylene groups of AMS sample. The main characteristic bands containing P-O_a (1068 cm^{-1}), M=O_d (969 cm^{-1}), $\text{M-O}_b\text{-M}$ (872 cm^{-1}) and $\text{M-O}_c\text{-M}$ (784 cm^{-1}) ($\text{M}=\text{W}, \text{Mo}$) indicated the formation of Keggin type structure of HPAs in Fig. 2c. Nevertheless, the blue shift of these bands for MW@AMS sample in comparison with pure MW is corresponded to strong interaction of MW with surface of support. The appearance of new band at 1451 cm^{-1} corresponding to NH_3^+ (Fig. 2d) confirmed ionic interaction between modified support and MW [31]. It is clear that the main characteristic bands of MW are retained and proved that Keggin structure is maintained in composite structure

and also the disappearance of amine group peak can be referred to interaction between NH_2 and MW [32].

In order to verify textural and morphology of synthesized samples scanning electron microscopy (SEM) and transmission electron microscopy (TEM) analysis are used. Fe_3O_4 nanoparticles as spherical shape with an average diameter of $100\text{--}140\text{ nm}$ are indicated in Fig. 2e. As seen, magnetic nanospheres have homogenous morphology although sticking of nanoparticles is observed in some areas that attributed to its high magnetic property. TEM images (Fig. 2f, g) revealed that iron oxide as a black core is coated by silica shell (is detected as bright grey shell) (Fig. 2f) that confirmed core–shell structure of synthesized nanocomposite and also these images indicated that the average length of channels is approximately 25 nm that arranged as a perpendicular to the surface of iron oxide particles. The MW species which include heavy atoms of molybdenum and tungsten are detected as dark grey particles in or outsides of SBA-15 channels (Fig. 2g).

Nitrogen adsorption–desorption technique is applied for determining of surface area and pores size distribution. Type IV isotherms are showed in Fig. 3a,b for both of them which classified for mesoporous materials. The inflection of the isotherms referred to the capillary condensation of nitrogen in mesopores with an H1 type hysteresis loop. As seen in Table S1, pore size of AMS is 5.3 nm and reaches to 7.6 nm for MW@AMS. The increased pore size is due to interaction between MW molecules that can form secondary pore structure and lead to a larger value of pore size [32]. Furthermore,

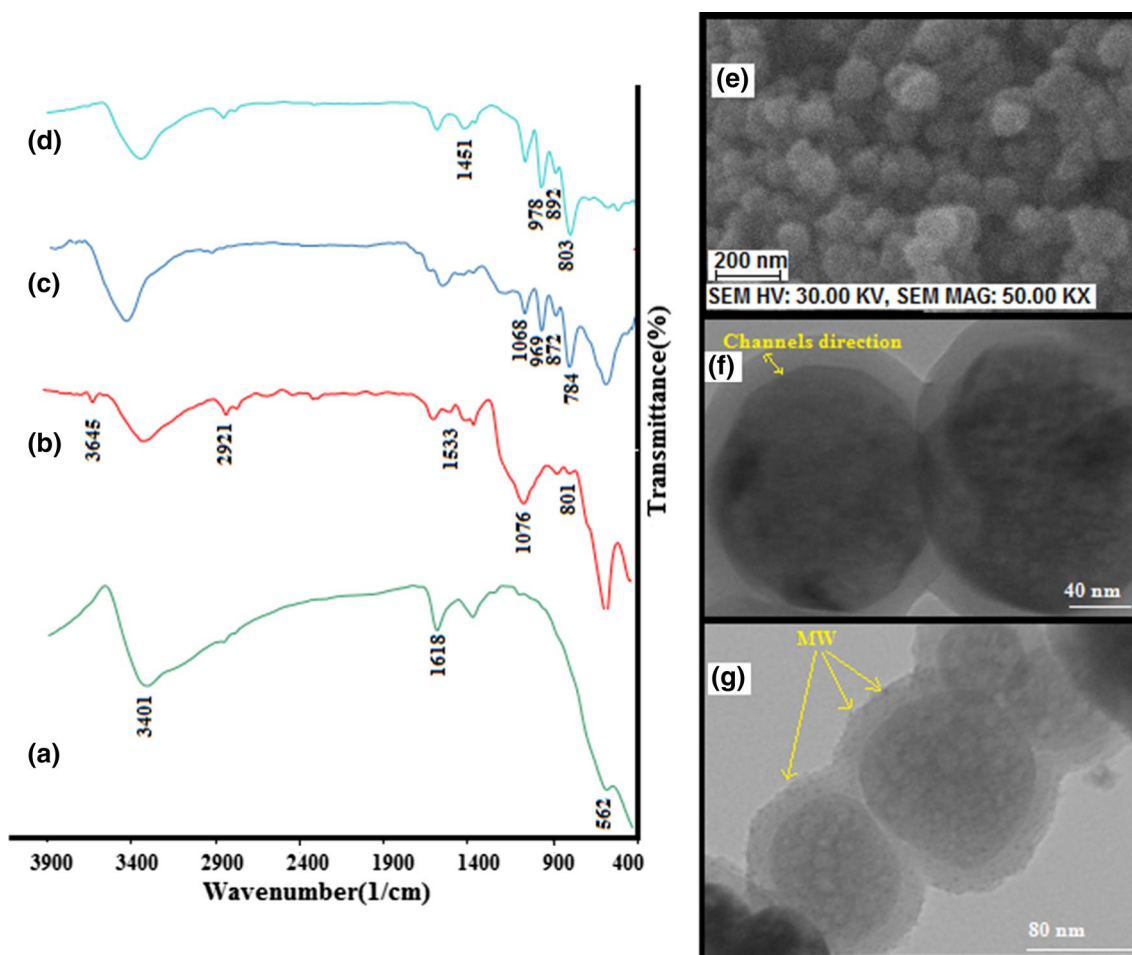


Fig. 2 FT-IR spectra of M (a), AMS (b), MW (c) MW@AMS (d), SEM images of the M (e), TEM image of AMS (f) and MW@AMS (g)

the BET surface area is decreased from 526.5 to 100.7 m²/g by loading of 25% MW which attributed to insert part of MW on the internal surface of mesoporous silica. Magnetic behavior of synthesized samples was measured by VSM analysis. Superparamagnetic property is verified for AMS and also MW@AMS at room temperature [33], whereas no hysteresis loop can be found in Fig. 3c. The saturated magnetization of AMS was 84.08 emu and declined to 16.23 emu for MW@AMS sample which this reduction can be corresponded to more presence of nonmagnetic particles in composite structure.

Adsorption tests

Effect of amount of loading on adsorption performance

One of the significant factors to evaluate the adsorbent capacity is an adsorbent dose. The adsorption efficiency as a function of adsorbent dose is indicated in Fig. 3d. In the experiments which AMS (without loading of MW) was

used, the removal efficiency of metal ions was only 44% and 41% for Co²⁺ and Sr²⁺ metal ions respectively that may be attributed to chelation of metal ions with amine and hydroxyl functional groups onto surface of support [31]. As seen; the removal efficiency is improved when loading percentage of MW increases and reaches to maximum value for 25% loading of MW. Adsorption efficiency is slightly diminished along with further increase loading that is probably due to blocking of accessible sites by agglomeration of species. The obtained results of Fig. 3d showed that approximately 40% of metal ions are uptaken by AMS sample. It is clear, in this step, complexation and physisorption processes were bold mechanisms that create by various functional groups in AMS support. However, adsorption efficiency reaches to maximum by introducing of MW (with excellent ion exchange properties) that confirms ion exchange is also involved mechanism in this system [30, 34]. In fact, the absorption of metals takes places by a set of processes.

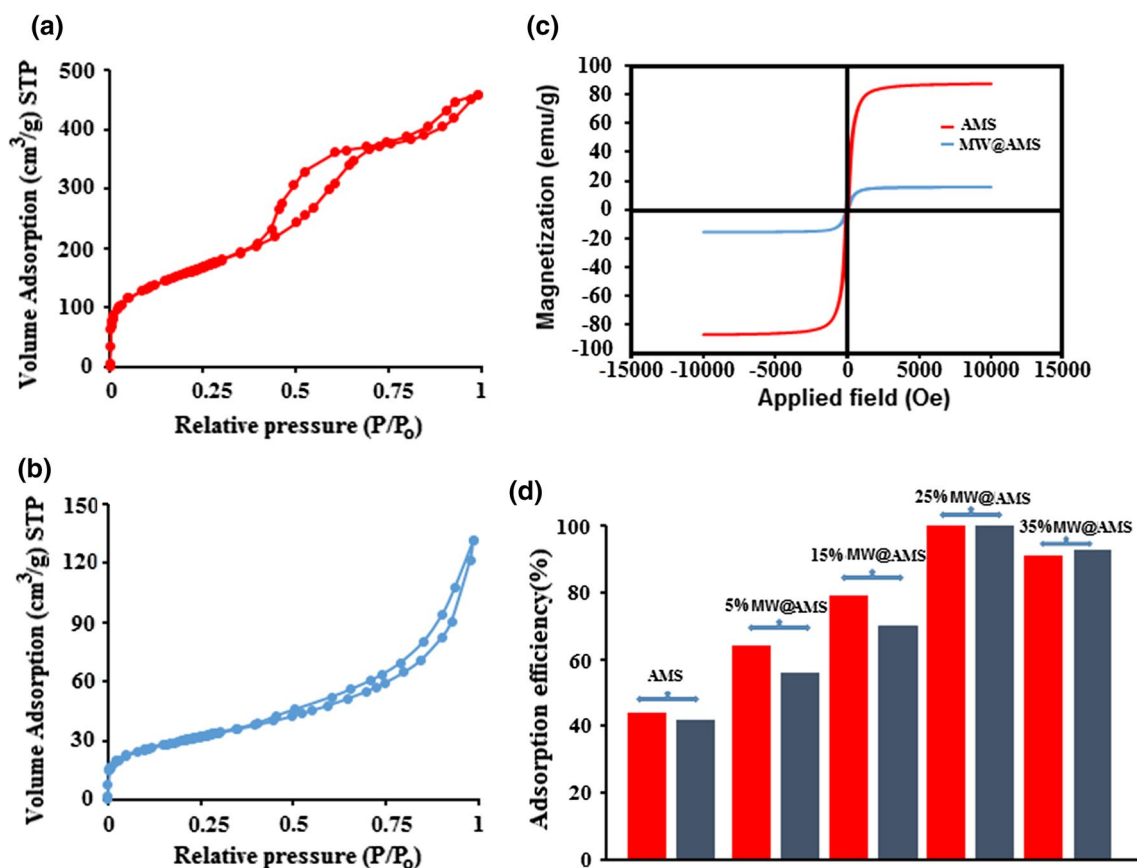


Fig. 3 N₂ adsorption–desorption isotherms of AMS (a), MW@AMS (b), magnetic hysteresis loops of AMS and MW@AMS (c) and adsorption efficiency for AMS, MW@AMS by various loading of MW (d)

The effect of pH

The pH of solution is an important factor in practical application of adsorbent. The pH adjustment of solution carried out by HNO₃ (0.1 M) and NaOH (0.1 M). At the different pH, metal ions exist in various form such as Co(OH)⁺, Co(OH)₂(s), Sr(OH)⁺ and Sr(OH)₂(s) that concentration of each of them depends on pH of solution. Co²⁺ and Sr²⁺ are dominant species at pH values range 1–6 and 1–13 respectively, while precipitate form become dominant species for both of them at higher pH values [35, 36]. As seen in Fig. 4a, the metal ions removal at low pH values is small, approximately 67% for Co²⁺ and 60% for Sr²⁺. However, removal efficiency slowly is improved by increasing pH. For more clarity of the subject, the pzc analysis was employed. At low pH, charge surface of composite is more positive that attributed to presence of protonated amine and hydroxyl groups on the surface support. However, it becomes more negative along with deprotonating of functional groups at

higher pH values (as seen in Fig. 4b). Furthermore, in this basic pH region, along with decreasing the H₃O⁺ ion, competitive adsorption between positive charge metal ion and H₃O⁺ is diminished for attraction on negative surface of adsorbent.

Effect of contact time

The investigation of contact time is a parameter that has significant effect on saving energy, time and money in the case of large scale process. For this purpose, the kinetic experiments were carried out by mixing 50 mg of composite with 20 mL of metal ion solution (C₀ = 10 mg L⁻¹). As seen (Fig. 5), the metal adsorption takes place rapidly in the first 60 min. This initial rapid uptake of metal ions referred to presence a lot of available active sites, following the equilibriums happened at 100 and 120 min for Co²⁺ and Sr²⁺ by gradual reduction of these sites and also increasing repulsive forces between cations formerly adsorbed with free positive ions in solution. The

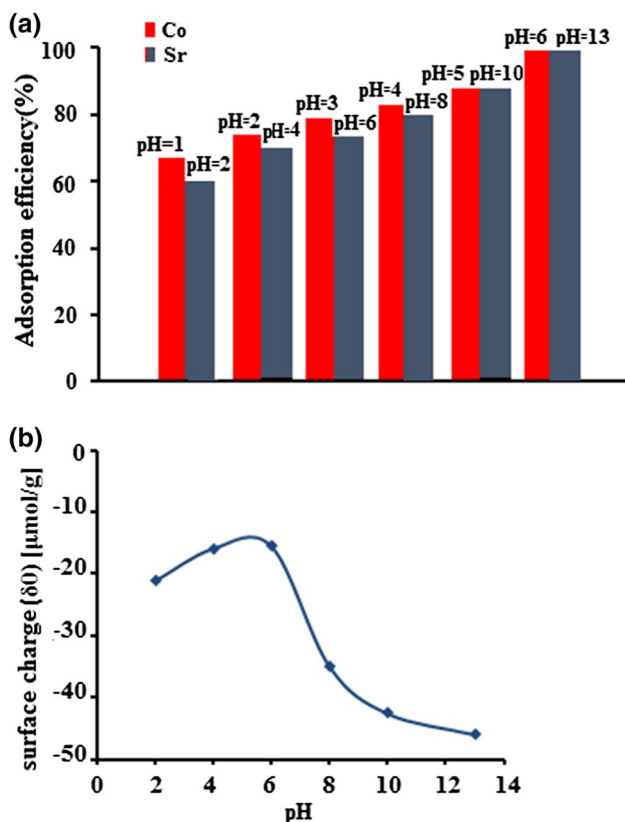


Fig. 4 The effect of pH solution on adsorption efficiency of Co²⁺ and Sr²⁺ (a), the surface charge versus pH for 25% MW@AMS sample (b)

kinetic adsorption of metal ions was evaluated using pseudo first-order and pseudo second-order models. A linear form of pseudo first-order equation (Eq. 3) [37] and pseudo second-order equation (Eq. 4) [38] are presented as

$$\log(q_e - q_t) = \log q_e - \frac{k_1 t}{2.303} \quad (3)$$

$$\frac{t}{q_t} = \frac{1}{k_2 q_e^2} + \frac{1}{q_e} t \quad (4)$$

where q_e and q_t were corresponded to metal ion adsorbed (mg g⁻¹) on the adsorbent at the equilibrium and at time t respectively, k_1 (L min⁻¹) and k_2 (g mg⁻¹ min⁻¹) are the pseudo first-order and the pseudo second-order rate constant of adsorption. By comparing data of Fig. 5 and Table S2, the pseudo second-order model was found to describe the adsorption process more effectively. Also, the results depicted a faster adsorption for Co ($k_2 = 1 \times 10^{-2}$) than Sr ($k_2 = 6 \times 10^{-3}$). Co²⁺ with smaller ion radius (70 pm) than Sr²⁺ (118 pm) [39] can diffuse easier and so it has an expander access to exchange sites that leads to its faster ion exchange capability.

Effect of initial metal ion concentration

To get a clear insight about mechanism of metal adsorption process and capacity of adsorbent, experimental tests were studied in range 10–200 ppm of metal ions concentration. As found from Fig. 6, the adsorption capacity is increased along with increase of metal ions until the adsorption equilibrium is achieved. The adsorption equilibrium curves were assayed by the Langmuir and Freundlich isotherms. The Langmuir model referred to a monolayer adsorption on a homogeneous surface, while Freundlich model assume a multilayer adsorption on a heterogeneous surface. These models are presented in form Eqs. 5 [40] and 6 [41] respectively

$$\frac{C_e}{q_e} = \frac{1}{b q_m} + \frac{C_e}{q_m} \quad (5)$$

$$\log q_e = \log k_f + \frac{1}{n} \log c_e \quad (6)$$

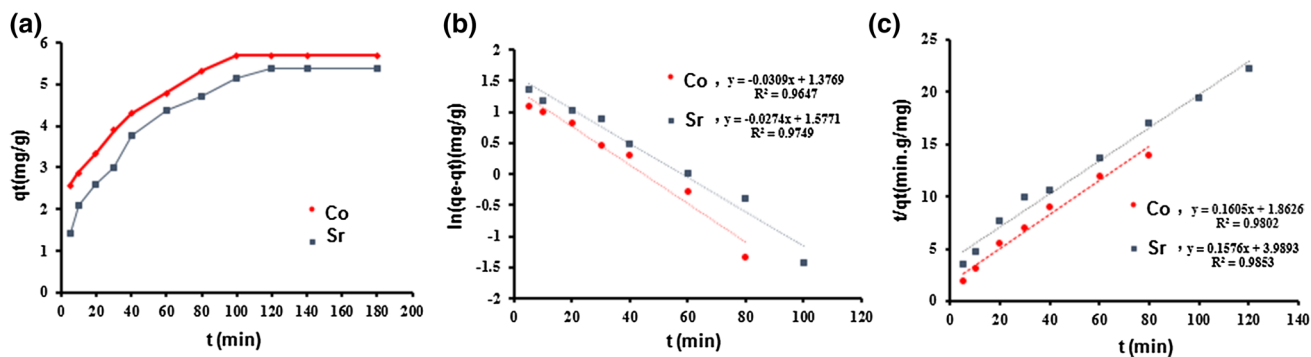


Fig. 5 Time dependence for Co²⁺ and Sr²⁺ adsorption (a), pseudo-first-order model fitting plots for Co²⁺ and Sr²⁺ adsorption kinetics data (b), pseudo-second-order model fitting plots for Co²⁺ and Sr²⁺ adsorption kinetics data (c)

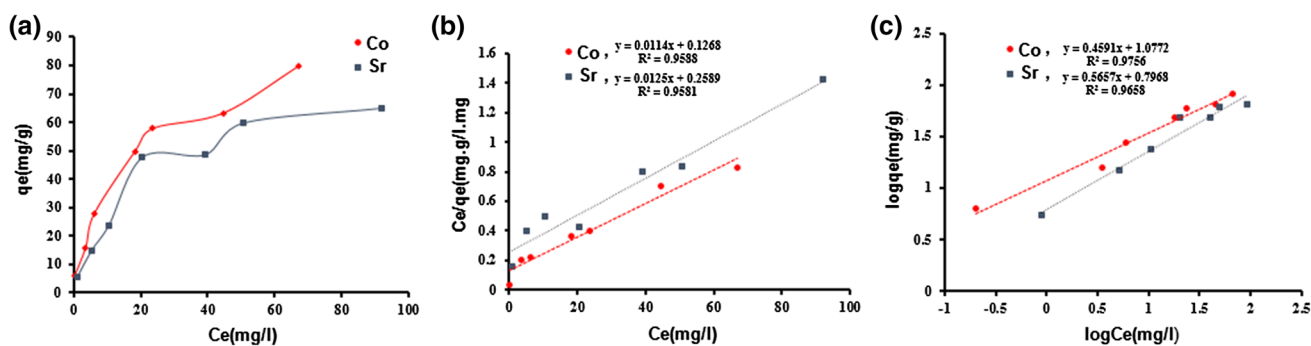


Fig. 6 Adsorption isotherm of 25% MW@AMS (a), linear Langmuir plot (b) and linear Freundlich plot (c)

where q_e is the adsorbed concentration of metal (mg g^{-1}) at equilibrium, b (L mg^{-1}) is a constant corresponded to energy of adsorption, q_m is the maximum adsorption capacity (mg g^{-1}), C_e is concentration of metal at equilibrium (mg L^{-1}), K_L and K_F are the Langmuir and Freundlich constant (L mg^{-1}) and $1/n$ (dimension less) referred to the heterogeneity factor. The obtained R^2 (Regression coefficients) of curve in Fig. 6b and c depicted that the Freundlich isotherm fitted better with experimental data than Langmuir. Based on Table S3, the calculated q_m are 87.72 and 80.01 mg g^{-1} for Co^{2+} and Sr^{2+} respectively.

For the better identify of the type sorption process (chemical or physical sorption), the Dubinin–Radushkevich (D–R) isotherm model was used. This isotherm model is shown as the following equation [42];

$$\ln(q_e) = \ln q_{\text{DR}} - B_{\text{DR}} \varepsilon^2 \quad (7)$$

where q_{DR} is the monolayer capacity (mmol g^{-1}), B_{DR} ($\text{mol}^2 \text{J}^{-2}$) is corresponded to adsorption energy and ε is the Polanyi potential which is determined by;

$$\varepsilon = RT \ln \left(1 + \frac{1}{C_e} \right) \quad (8)$$

where R is the gas universal constant ($8.314 \text{ J mol}^{-1} \text{ K}^{-1}$) and T is referred to the absolute temperature (K). The main parameters of (D–R) equation to estimate the type of sorption process is obtained by measuring of the value of mean free energy for per molecule of adsorbate [E (kJ mol^{-1})] as below:

$$E = \frac{1}{\sqrt{2B_{\text{DR}}}} \quad (9)$$

If value of E was less than 8 kJ mol^{-1} , the physical sorption is considered as mainly mechanism and the chemical sorption will be expected if value of E was $8\text{--}16 \text{ kJ mol}^{-1}$. The obtained data of Fig. 7a are tabulated in Table S4. Whereas the values of E are placed between 1 and 8, physical attraction can be affected on metal ions sorption. The

adsorption capacity by 25%MW@AMS and other adsorbents indicated in Table S5. As observed, 25%MW@AMS composite has an excellent potential for uptake of Co^{2+} and Sr^{2+} .

Effect of temperature

To study the thermodynamic behavior of the adsorption system, temperature of solution adjusted at 25, 35, 45 and 55°C (under optimum condition found). As observed, adsorption efficiency was increased with rising in temperature (Fig. 7b) that can be attributed to improved transport of metal ions from the bulk to the surface phase along with increasing temperature [63]. The thermodynamic parameters can be calculated by plotting of $\ln K_c$ versus $1/T$.

$$\ln K_c = \frac{\Delta S^\circ}{R} - \frac{\Delta H^\circ}{RT} \quad (10)$$

where K_c is referred to thermodynamic equilibrium constant, T (K) is temperature and R is universal gas constant ($8.314 \text{ J mol}^{-1} \text{ K}^{-1}$). According to Vant Hoff equation (Eq. 11) [64], the standard free energy change G (kJ mol^{-1}) is calculated as shown below:

$$\Delta G^\circ = \Delta H^\circ - T\Delta S^\circ \quad (11)$$

All parameters tabulated in Table S6. The negative values of ΔG° at all temperatures indicated the spontaneous nature of this process and endothermic behavior resulted in positive value for ΔH° . Generally, if $0 < \Delta G < -20 \text{ kJ mol}^{-1}$, physical adsorption is dominant and changes to more negative values than -40 kJ mol^{-1} for chemical adsorption [65]. The obtained ΔG° at all temperatures are between 0 and -20 kJ mol^{-1} that referred to physical adsorption and in accordance with gained result of Dubinin–Radushkevich model. The positive values of ΔS were reflected an increased degree of randomness at the solid/solution interface that are interpreted with exchange of bivalent metal ions along with freedom of two hydrogen ions in solution and confirmed by the change of pH to lower values.

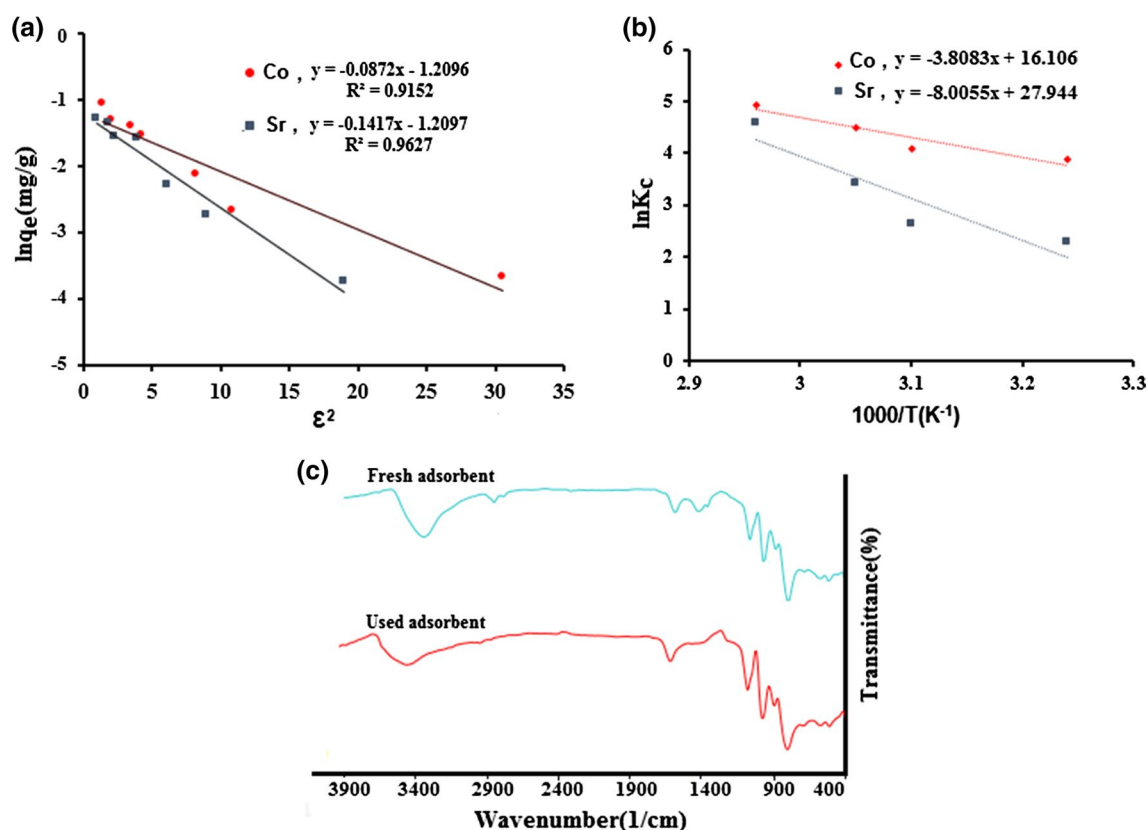


Fig. 7 The Dubin–Radushkevich isotherm for adsorption of Co^{2+} and Sr^{2+} by 25% MW@AMS (a), the effect of temperature on adsorption of Co^{2+} and Sr^{2+} ions (b) and FT-IR spectra of fresh and used adsorbent (c)

Desorption and reusability of adsorbent

The investigation of stability and reusability of adsorbent is an essential step in designing effective and economic system for treatment of polluted solution. The FT-IR and ICP analyses are employed for investigation of stability of adsorbent. In Fig. 7c, FT-IR spectra indicated that the characteristic peaks of MW and ASM are preserved in the composite structure of the used adsorbent. Also, the obtained data of ICP analysis revealed that only less than 3% of MW leached after four running cycles. To explore reusability, the adsorption–desorption test was carried out for four consecutive cycles. In each cases, the used adsorbent was separated and washed with elution agents and again employed in adsorption process. 0.1 M HCl and 0.1 M EDTA were used as elution agents. Adsorption efficiency slightly reduced after four cycles resulting a good reusability of the adsorbent (Fig. 8). As seen in Fig. 8 and Table S7, EDTA had a better desorption and regeneration efficiency in comparison with HCl. This result can be attributed to larger chelating stability constant of EDTA with Co^{2+} and Sr^{2+} than HCl [61].

Chemical stability of adsorbent

The adsorbent (0.05 g) was placed separately in 10 mL of different solvents at room temperature for 12 h and then separated. Molybdenum in the filtrate were determined (Table S8). The adsorbent indicates excellent chemical stability toward acids, alkali and water. Hence these ion exchangers can be utilized in most of the aqueous media without leaching problems.

Conclusion

In this work, MW@AMS was synthesized for the first time, perfectly characterized and was employed for removal of Co^{2+} and Sr^{2+} metal ions from aqueous solution. The obtained results revealed that the adsorption isotherms well obeyed Freundlich model with maximum sorption capacity of 87.72 mg g^{-1} and 80.01 mg g^{-1} for Co^{2+} and Sr^{2+} ions respectively. The obtained values of Gibbs free energy change (G) and enthalpy change (H) indicated spontaneous nature and endothermic behavior of

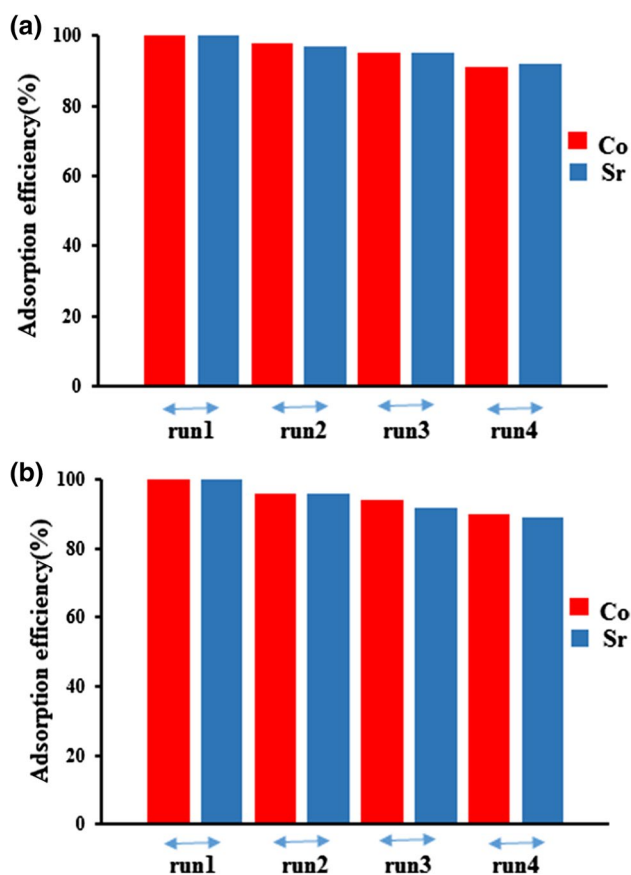


Fig. 8 Adsorption efficiency of Co²⁺ and Sr²⁺ ions versus adsorbent recycled runs using EDTA (a) and HCl (b)

adsorption process. EDTA with larger chelating stability constant in comparison with HCl demonstrated a better desorption and regeneration efficiency. This adsorbent was isolated easily and quickly with an external magnetic, so it can be considered as effective and economical adsorbent for treatment of polluted solution.

Acknowledgements The financial support of this study by Tarbiat Modares university is gratefully acknowledged.

References

- Lin L, Xu X, Papelis C, Xu P (2017) Innovative use of drinking water treatment solids for heavy metals removal from desalination concentrate: synergistic effect of salts and natural organic matter. *Chem Eng Res Des* 120:231–239
- Sun YB, Wang XX, Ding CC, Cheng WC, Chen CL, Hayat T, Alsaedi A, Hu J, Wang X (2016) Direct synthesis of bacteria-derived carbonaceous nanofibers as a highly efficient material for radionuclides elimination. *ACS Sustain Chem Eng* 4:4608–4616
- Chen Y, Wang J (2012) Removal of radionuclide Sr²⁺ ions from aqueous solution using synthesized magnetic chitosan beads. *Nucl Eng Des* 242:445–451
- El-Wakil MM (1988) Powerplant technology. Tata McGraw-Hill Education, New York
- He M, Zhu Y, Yang Y, Han B, Zhang Y (2011) Adsorption of cobalt (II) ions from aqueous solutions by palygorskite. *Appl Clay Sci* 54:292–296
- Toxic Substances and Disease Registry (ATSDR) (2004) Toxicological profile for cobalt. U.S. Department of Health and Human Services, Atlanta
- Jiao J, Zhao J, Pei Y (2017) Adsorption of Co(II) from aqueous solutions by water treatment residuals. *J Environ Sci* 52:232–239
- Aryal M, Liakopoulou-Kyriakides M (2015) Bioremoval of heavy metals by bacterial biomass. *Environ Monit Assess* 187:4173
- Chen G, Shah KJ, Shi L, Chiang PC (2017) Removal of Cd(II) and Pb(II) ions from aqueous solutions by synthetic mineral adsorbent: performance and mechanisms. *Appl Surf Sci* 409:296–305
- Li F, Chen Y, Huang H, Cao W, Li T (2015) Removal of rhodamine B and Cr(VI) from aqueous solutions by a polyoxometalate adsorbent. *Chem Eng Res Des* 100:192–202
- Park Y, Shin WS, Choi SJ (2013) Calcined graphene/MgAl-layered double hydroxides for enhanced Cr(VI) removal. *Chem Eng J* 220:204–213
- Long DL, Tsunashima R, Cronin L (2010) Polyoxometalates: building blocks for functional nanoscale systems. *Angew Chem Int Ed* 49:1736–1758
- Chamack M, Mahjoub AR, Aghayan H (2015) Catalytic performance of vanadium-substituted molybdophosphoric acid supported on zirconium modified mesoporous silica in oxidative desulfurization. *Chem Eng Res Des* 94:565–572
- Granadeiro CM, Ribeiro SO, Kaczmarek AM, Cunha-Silva L, Almeida PL, Gago S, Deun RV, Castro B, Balula SS (2016) A novel red emitting material based on polyoxometalate@ periodic mesoporous organosilica. *Microporous Mesoporous Mater* 234:248–256
- Pourbeyram S, Moosavifar M, Hasanzadeh V (2014) Electrochemical characterization of the encapsulated polyoxometalates (POMs) into the zeolite. *J Electroanal Chem* 714–715:19–24
- Ucar A, Findik M, Gubbuk IH, Kocak N, Bingol H (2017) Catalytic degradation of organic dye using reduced graphene oxide-polyoxometalate nanocomposite. *Mater Chem Phys* 196:21–28
- Bai Z, Zhou C, Xu H, Wang G, Pang H, Ma H (2017) Polyoxometalates-doped Au nanoparticles and reduced graphene oxide: a new material for the detection of uric acid in urine. *Sens Actuators, B* 243:361–371
- Lei D, Zheng Q, Wang Y, Wang H (2015) Preparation and evaluation of aminopropyl-functionalized manganese-loaded SBA-15 for copper removal from aqueous solution. *J Environ Sci* 28:118–127
- Masteri-Farahani M, Modarres M (2016) Wells-Dawson heteropoly acid immobilized inside the nanocages of SBA-16 with ship-in-a-bottle method: a new recoverable catalyst for the epoxidation of olefins. *J Mol Catal A: Chem* 417:81–88
- Park Y, Shin WS, Choi SJ (2013) Ammonium salt of heteropoly acid immobilized on mesoporous silica (SBA-15): an efficient ion exchanger for cesium ion. *Chem Eng J* 220:204–213
- Srivastava S, Agrawal SB, Mondal MK (2017) Synthesis, characterization and application of *Lagerstroemia speciosa* embedded magnetic nanoparticle for Cr(VI) adsorption from aqueous solution. *J Environ Sci* 55:283–293
- Zheng X, Dou J, Yuan J, Qin W, Hong X, Ding A (2017) Removal of Cs⁺ from water and soil by ammonium-pillared montmorillonite/Fe₃O₄ composite. *J Environ Sci* 56:12–24
- Wang Q, Li Y, Liu B, Dong Q, Xu G, Zhangab L, Zhang J (2015) Novel recyclable dual-heterostructured Fe₃O₄@CeO₂/M (M = Pt, Pd and Pt–Pd) catalysts: synergistic and redox effects for superior catalytic performance. *J Mater Chem A* 3:139–147

24. Li W, Zhang B, Li X, Zhang H, Zhang Q (2013) Preparation and characterization of novel immobilized $\text{Fe}_3\text{O}_4@\text{SiO}_2@m\text{SiO}_2$ -Pd(0) catalyst with large pore-size mesoporous for Suzuki coupling reaction. *Appl Catal A* 459:65–72
25. Huixiong W, Mei Z, Yixin Q, Haixia L, Hengbo Y (2009) Preparation and characterization of tungsten-substituted molybdophosphoric acids and catalytic cyclodehydration of 1,4-butanediol to tetrahydrofuran. *Chin J Chem Eng* 17:200–206
26. Berger D, Georgescu D, Bajenaru L, Zanfir A, Stănică N, Matei C (2017) Properties of mesostructured silica coated CoFe_2O_4 versus Fe_3O_4 -silica composites. *J Alloys Compd* 708:278–284
27. Fumin Z, Chaoshu Y, Jun W, Yan K, Haiyang Z, Chunyan W (2006) Synthesis of fructose over dealuminated USY supported heteropoly acid and its salt catalysts. *J Mol Catal A: Chem* 247:130–137
28. Yavari R, Ahmadi SJ, Huang YD, Khanchi AR, Bagheri G, He JM (2009) Synthesis, characterization and analytical application of a new inorganic cation exchanger—Titanium(IV) molybdophosphate. *Talanta* 77:1179–1184
29. Mardiroosi A, Mahjoub AR, Fakhri H (2017) Efficient visible light photocatalytic activity based on magnetic graphene oxide decorated ZnO/NiO. *J Mater Sci: Mater Electron* 28:11722–11732
30. Ghorbani M, Nowee SM, Ramezani N, Raji F (2016) A new nanostructured material amino functionalized mesoporous silica synthesized via co-condensation method for Pb(II) and Ni(II) ion sorption from aqueous solution. *Hydrometallurgy* 161:117–126
31. Shaker MA (2015) Adsorption of Co(II), Ni(II) and Cu(II) ions onto chitosan-modified poly(methacrylate) nanoparticles: dynamics, equilibrium and thermodynamics studies. *J Taiwan Inst Chem Eng* 57:111–122
32. Zhao L, Chi Y, Yuan Q, Li N, Yan W, Li X (2013) Phosphotungstic acid anchored to amino-functionalized core-shell magnetic mesoporous silica microspheres: a magnetically recoverable nanocomposite with enhanced photocatalytic activity. *J Colloid Interface Sci* 390:70–77
33. Zhang YL, Zhang J, Dai CM, Zhou XF, Liu SG (2013) Sorption of carbamazepine from water by magnetic molecularly imprinted polymers based on chitosan- Fe_3O_4 . *Carbohydr Polym* 97:809–816
34. Fakhri H, Mahjoub AR, Aghayan H (2017) Effective removal of methylene blue and cerium by a novel pair set of heteropoly acids based functionalized graphene oxide: adsorption and photocatalytic study. *Chem Eng Res Des* 120:303–315
35. Zhang L, Wei J, Zhao X, Li F, Jiang F, Zhang M, Cheng X (2016) Competitive adsorption of strontium and cobalt onto tin antimonite. *Chem Eng J* 285:679–689
36. Kyzas GZ, Deliyanni EA, Matis KA (2016) Activated carbons produced by pyrolysis of waste potato peels: cobalt ions removal by adsorption. *Colloids Surf A* 490:74–83
37. Lagergren S (1898) Zur theorie der sogenannten adsorption gelöster stoffe. *Kungliga Svenska Vetenskapsakademiens. Handlingar* 24:1–39
38. Ho Y (2006) Review of second-order models for adsorption systems. *J Hazard Mater B* 136:681–689
39. Web elements periodic table of the elements. The University of Sheffield and Web Elements Ltd, UK. <http://www.wiredchemist.com/chemistry/data/metallic-radial> (1993–2017)
40. Langmuir I (1918) The adsorption of gases on plane surfaces of glass, mica and platinum. *JACS* 40:1361–1403
41. Gunten UV (2003) Ozonation of drinking water: part I. Oxidation kinetics and product formation. *Water Res* 37:1443–1467
42. Dubinin MM (1960) The potential theory of adsorption of gases and vapors for adsorbents with energetically non-uniform surface. *Chem Rev* 60:235–266
43. He M, Zhu Y, Yang Y, Han B, Zhang Y (2011) Adsorption of cobalt(II) ions from aqueous solutions by palygorskite. *Appl Clay Sci* 54:292–296
44. Zhang L, Wei J, Zhao X, Li F, Jiang F, Zhang M, Cheng X (2016) Competitive adsorption of strontium and cobalt onto tin antimonite. *Chem Eng J* 285:679–689
45. Dotto GL, Cunha JM, Calgareo CO, Tanabe EH, Bertuol DA (2015) Surface modification of chitin using ultrasound-assisted and supercritical CO_2 technologies for cobalt adsorption. *J Hazard Mater* 295:29–36
46. Hadi P, Barford J, McKay G (2013) Synergistic effect in the simultaneous removal of binary cobalt-nickel heavy metals from effluents by a novel e-waste-derived material. *Chem Eng J* 228:140–146
47. Tayyebi A, Outokesh M, Moradi S, Doram A (2015) Synthesis and characterization of ultrasound assisted “grapheneoxide-magnetite” hybrid, and investigation of its adsorption properties for Sr(II) and Co(II) ions. *Appl Surf Sci* 353:350–362
48. Cheng R, Kang M, Zhuang S, Shi L, Zheng X, Wang J (2019) Adsorption of Sr(II) from water by mercerized bacterial cellulose membrane modified with EDTA. *J Hazard Mater* 364:645–653
49. Li M, Liu H, Zhu H, Gao H, Zhang S, Chen T (2017) Kinetics and mechanism of Sr(II) adsorption by Al- Fe_2O_3 : evidence from XPS analysis. *J Mol Liq* 233:364–369
50. Abdel-Karim AAM, Zaki AA, Elwan W, El-Naggar MR, Gouda MM (2016) Experimental and modeling investigations of cesium and strontium adsorption onto clay of radioactive waste disposal. *Appl Clay Sci* 132–133:391–401
51. Zhang L, Wei J, Zhao X, Li F, Jiang F (2015) Adsorption characteristics of strontium on synthesized antimony silicate. *Chem Eng J* 277:378–387
52. Zhang L, Wei J, Zhao X, Li F, Jiang F, Zhang M (2015) Strontium (II) adsorption on Sb(III)/Sb $_2\text{O}_5$. *Chem Eng J* 267:245–252
53. Inan S, Nostar E (2013) Structure and ion exchange behavior of zirconium antimonates for strontium. *Sep Sci Technol* 48:1364–1369
54. İnan S, Altaş Y (2010) Adsorption of strontium from acidic waste solution by Mn-Zr mixed hydrous oxide prepared by co-precipitation. *Sep Sci Technol* 45:269–276
55. Guan W, Pan J, Ou H, Wang X, Zou X, Hu W, Li C, Wu X (2011) Removal of strontium (II) ions by potassium tetratitanate whisker and sodium trititanate whisker from aqueous solution: equilibrium, kinetics and thermodynamics. *Chem Eng J* 167:215–222
56. Javed MA, Bhatti HN, Hanif NA, Nadeem R (2007) Kinetic and equilibrium modeling of Pb(II) and Co(II) Sorption onto rose waste biomass. *Sep Sci Technol* 42:3641–3656
57. Olgun A, Atar N (2011) Removal of copper and cobalt from aqueous solution onto waste containing boron impurity. *Chem Eng J* 167:140–147
58. Manohar DM, Noeline BF, Anirudhan TS (2006) Adsorption performance of Al-pillared bentonite clay for the removal of cobalt (II) from aqueous phase. *Appl Clay Sci* 31:194–206
59. Ivanets AI, Katsoshvili LL, Krivoschapkin PV, Prozorovich VG, Kuznetsova TF, Krivoschapkina EF, Radkevich AV, Zarubo AM (2017) Sorption of strontium ions onto mesoporous manganese oxide of OMS-2 type. *Radiochemistry* 59:264–271
60. Ivanets AI, Shashkova IL, Kitikova NV, Drozdova NV (2014) Extraction of Co(II) Ions from aqueous solutions with thermally activated dolomite. *Russ J Appl Chem* 87:270–275
61. Ivanets AI, Prozorovich VG, Kouznetsova TF, Radkevich AV, Krivoschapkin PV, Krivoschapkina EF, Sillanpää M (2018) Sorption behavior of ^{85}Sr onto manganese oxides with tunnel structure. *J Radioanal Nucl Chem* 316:673–683
62. Ivanets AI, Srivastava V, Roshchina MY, Sillanpää M, Prozorovich VG, Pankov VV (2018) Magnesium ferrite nanoparticles as a magnetic sorbent for the removal of Mn^{2+} , Co^{2+} , Ni^{2+} and Cu^{2+} from aqueous solution. *Ceram Int* 44:9097–9104
63. Cheng C, Wang J, Yang X, Li A, Philippe C (2014) Adsorption of Ni(II) and Cd(II) from water by novel chelating sponge and the

- effect of alkali-earth metal ions on the adsorption. *J Hazard Mater* 264:332–341
64. Rajic N, Stojakovic D, Jovanovic M, Logar NZ, Mazaj M, Kaucic V (2010) Removal of nickel (II) ions from aqueous solutions using the natural clinoptilolite and preparation of nano-NiO on the exhausted clinoptilolite. *Appl Surf Sci* 257:1524–1532
65. Liu X, Luo J, Zhu Y, Yang Y, Yang S (2015) Removal of methylene blue from aqueous solutions by an adsorbent based on metal-organic framework and polyoxometalate. *J Alloys Compd* 648:986–993

Publisher's Note Springer Nature remains neutral with regard to jurisdictional claims in published maps and institutional affiliations.